Liquid Crystals
Publication details, including instructions for authors and subscription information:
http://www.informaworld.com/smpp/title~content=t713926090

Artificial enzymes based on imprinted liquid-crystalline materials

M. Weyland[a]; S. Ferrère[a]; A. Lattes[a]; A. -F. Mingotaud[a]; M. Mauzac[a]
[a] Laboritoire des Interactions Moléculaires et Réactivité Chimique et Photochimique, UMR CNRS 5623, Université Paul Sabatier, 31062 Toulouse cedex 9, France

First published on: 13 December 2007

To cite this Article Weyland, M. , Ferrère, S. , Lattes, A. , Mingotaud, A. -F. and Mauzac, M.(2008) 'Artificial enzymes based on imprinted liquid-crystalline materials', Liquid Crystals, 35: 2, 219 — 231, First published on: 13 December 2007 (iFirst)
To link to this Article: DOI: 10.1080/02678290701751566
URL: http://dx.doi.org/10.1080/02678290701751566

Liquid Crystals,
Vol. 35, No. 2, February 2008, 219–231

Taylor & Francis
Taylor & Francis Group

Artificial enzymes based on imprinted liquid-crystalline materials

M. Weyland, S. Ferrère, A. Lattes, A.-F. Mingotaud* and M. Mauzac

Laboritoire des Interactions Moléculaires et Réactivité Chimique et Photochimique, UMR CNRS 5623, Université Paul Sabatier, 118 Route de Narbonne, 31062 Toulouse cedex 9, France

(Received 27 June 2007; final form 26 September 2007)

Liquid-crystal elastomers, imprinted around indole, are assessed as artificial enzymes for the isomerisation of benzisoxazole into 2-cyano phenol. Two types of material are synthesised, tested in the catalysis and compared with non-liquid-crystal imprinted polymers: an imprinted liquid-crystalline elastomer and a semi-interpenetrated imprinted liquid-crystal network. The catalytic effect of all materials is close. However, the main benefit for the liquid-crystal elastomer is shown to be the shape memory of the material at the molecular scale, because the isomerisation kinetics are found to be identical before and after deformation of the cavities either by thermal treatment up to the isotropic state or by solvent induced swelling. This fact is related to the coupling between the order and the conformation of the polymer chains, which is fixed by the crosslinking process. On the other hand, the imprinted sites of the semi-interpenetrated imprinted liquid-crystal elastomer are shown to be almost 100 times more active than the non-imprinted sites in the catalysis. This factor is only 22 for the corresponding non-liquid-crystalline network.

Keywords: elastomers; enzymes; liquid-crystalline polymers; molecular imprinting; semi-interpenetrated networks

1. Introduction

The so-called molecularly imprinted polymers (MIPs) mimic the molecular recognition phenomena present in living systems. These are synthesised (Scheme 1) by polymerising and crosslinking monomers in interaction with a chosen template (*1, 2*). The interactions between the template and the monomers can be either covalent or non-covalent. In the latter case, the first step consists of forming the complex between both molecules, which has to be stable during the polymerisation and crosslinking. After removal of the template by washing steps, the material presents specific cavities that are complementary in shape and size. Most of the drawbacks of this method have been linked to the need for a large amount of crosslinking agent (usually around 80–90%) to restrict distortion phenomena of the polymer backbones. In order to overcome this problem, we have recently developed new MIPs using liquid-crystal elastomers (*3*). Owing to the physical crosslinking due to the mesogens, low chemical crosslinking (around 5%) has been found to be sufficient to keep the shape of the cavities in the MIP. By this technique, new materials that have similar selectivity but much higher capacity compared with classical MIPs have been made available. In our continuing studies on this subject, we were interested in determining the usefulness of such molecular imprinted liquid-crystalline elastomers as artificial enzymes. Indeed, when the chosen template is a stable transition-state analogue of a reaction, the molecular imprinted materials obtained from this after removal of the template can act as a catalyst for this reaction, therefore resembling the action of natural enzymes. This technique has been tested for several years now and several recent reviews can be found in the literature (*1, 2, 4, 5*). Various reactions have been catalysed in this way: elimination (*6–8*), C–C bond formation (*9–11*), oxidation or reduction (*12–14*) and, mainly, hydrolysis of esters or carbonates (*15–21*). The efficiency of the imprint on the catalysis can be described by comparing the kinetics of the MIP with the kinetics of a material synthesised with the same molecules (including the monomer that interacts with the template) but without the template. From this point of view, very efficient systems begin to appear, the most outstanding at this time being the case of the hydrolysis of carbonate molecules where the reaction has been accelerated by a factor of 50–80 in the presence of the MIP (*17*). These ratios become quite close to what can be obtained by bioimprinting, which uses denatured proteins as MIPs (*22, 23*).

In order to determine the behaviour of liquid-crystal MIPs in such catalysis, we decided to start from an existing study and reproduce it with liquid-crystal imprinted materials. The case that we chose described benzisoxazole isomerisation into 2-cyano phenol carried out by Liu and Mosbach (*8*) (Scheme 2). In their article, the chosen template was indole, because of its commercial availability and its ability to mimic the departing proton in the transition

*Corresponding author. Email: afmingo@chimie.ups-tlse.fr

ISSN 0267-8292 print/ISSN 1366-5855 online

DOI: 10.1080/02678290701751566
http://www.informaworld.com

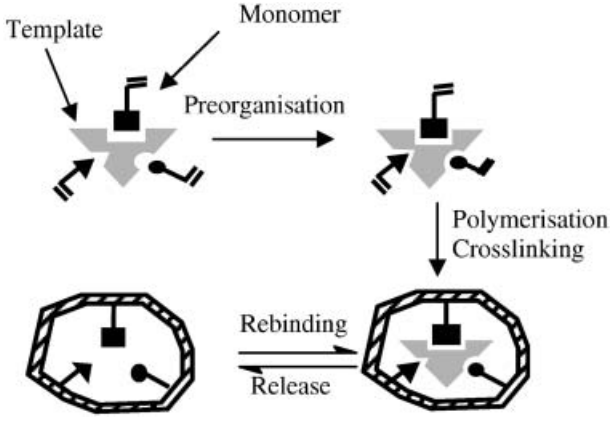

Scheme 1. Molecular imprinting technique.

state. The MIP consisted of a network of 85 mol% ethyleneglycoldimethacrylate (EGDMA) with specific cavities containing pendent pyridine groups coming from 4-vinylpyridine (4-VP) monomers (15 mol%). The network was synthesised by radical polymerisation, photoinitiated at 4°C. The observed acceleration of the MIP compared with a non-imprinted material (v_{MIP}/v_{NIP}) was found to be close to 7.

We decided to test two types of imprinted liquid-crystal material: a simple elastomer and a semi-interpenetrated network (s-IPN). The classical s-IPNs consist of a regular linear polymer that is entangled in a totally distinct polymer network. This kind of material has been shown to be very useful in improving the properties of polymer blends that otherwise would not be miscible. Only a few studies have examined the possibility of using s-IPNs for MIPs. A first example was reported in 1998 by Sreenivasan (*24*) who described the synthesis of a hydroxyethylmethacrylate network around a polyurethane polymer in the presence of cholesterol. This material exhibited good selectivity for cholesterol and was presented as a good candidate for a MIP membrane. In a more recent article (*25*), the molecular imprinting of haemoglobin was performed by incorporating chitosan in a methacrylamide network. The s-IPN was shown to exhibit a much higher adsorption capacity for haemoglobin compared with a non-imprinted material and also a higher selectivity. Descriptions of s-IPNs based on liquid-crystal polymers have also been rare. Zhao *et al.* described the trapping of a liquid-crystalline polymer in crosslinked polyacrylonitrile or polystyrene (*26–28*). They mostly investigated the compatibilisation effect and did not examine whether the resulting s-IPN was still liquid crystalline or not. In addition to this work, Zentel and colleagues have also used s-IPNs to obtain highly crosslinked materials with the capacity to keep the liquid-crystalline order (*29, 30*).

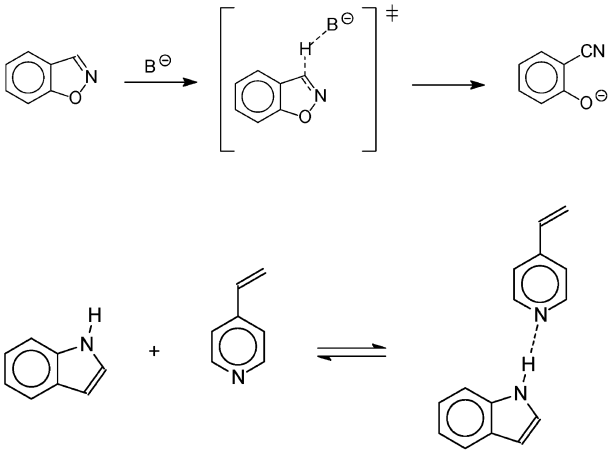

Scheme 2. Base-catalysed isomerisation of benzisoxazole and complex formation between indole and 4-VP.

2. Experimental details

2.1. Materials

Monomers MAC6OMe (4′-(6-methacryloyloxyhexyloxy)phenyl-4(methoxy) benzoate) and MAC6CN (4-cyano-4′(6-methacryloyloxyhexyloxy) biphenyl) were synthesised according to already published procedures (*3, 31–33*). MAC6OMe is a monotropic liquid crystal with an isotropic to nematic transition at 34°C. MAC6CN is not liquid crystalline and presents only a melting temperature at 79.7°C. However, the corresponding polymer has been shown to be liquid crystalline (*33, 34*). 2,2′-Azodiisobutyronitrile (AIBN), EGDMA and indole (Aldrich) were used without further purification. 4-VP (Aldrich) was dried over KOH, trap-to-trap distilled and kept under vacuum in a freezer. Benzisoxazole (BziO) was distilled just before use to ensure that no trace of 2-cyanophenol was present. All solvents were reagent grade and used without purification. They were degassed under nitrogen or argon for 30 min when needed.

2.2. Instruments

Proton nuclear magnetic resonance (^{1}H NMR) spectra were recorded on a Bruker Avance 300 spectrometer at 300.13 MHz at 4°C or at room temperature. Two-dimensional nuclear overhauser effect spectroscopy (NOESY) experiments were recorded on a Bruker Avance 500 at 500.13 MHz. $CDCl_3$ was used as the solvent. Infrared (IR) spectra were recorded on a Perkin-Elmer IR FT 1760-X.

Radical polymerisation was initiated with a 500 W xenon lamp equipped with a dichroid mirror and a WG 335 UV Oriel filter, in order to select only the wavelengths that are between 335 and 650 nm. Light was delivered to the reaction vessel through an optical fibre and its intensity was 19 mW cm^{-2}. The distance between the tip of the optical fibre and the sample was fixed at 3.3 cm.

The average molecular weight of the linear polymers was determined by size exclusion chromatography in tetrahydrofuran (THF; flow rate 1.2 ml min^{-1}) on an apparatus equipped with a Waters refractive index detector, a Waters column pack (Ultrastyragel 10^4, 10^3, 100 Å) and a Minidawn Wyatt light scattering detector. The refractive index increment for poly(MAC6CN-co-4-VP) (82/18 mol%) was measured and found at 0.246 ml g^{-1}.

Polymer particles were crushed in a liquid nitrogen grinder (Spex freezer mill) between 3 and 5 min and sifted with an AS 200 basic Retsch apparatus operated with four sieves (25, 75, 125 and 180 µm). Sieving time was set to 10 min. Differential scanning calorimetry (DSC) experiments were carried out on a Perkin Elmer Pyris 1 instrument. The temperature rate was 10°C min^{-1} on either heating or cooling ramps. Transition temperatures were measured on the second heating cycles.

Polarised optical microscopy (POM) was performed on an Olympus BX 50 with $\times 100$ or $\times 200$ lenses. High-performance liquid chromatography (HPLC) titration was performed on a Waters Alliance 2695 apparatus, equipped with a UV detector Waters 2487. Products were detected at $\lambda = 270$ nm. The column was a Waters XTerra RP 18 and an eluent gradient was applied from water/CH_3CN 55/45 to pure acetonitrile. Scanning electron microscopy (SEM) was carried out on a Hitachi S450 instrument (Centre de microscopie électronique appliquée à la biologie, Toulouse). The particles were metallised with a JFC 1100 Jeol apparatus for 5 m and a deposition speed of 100 nm min^{-1}.

2.3. Methods

2.3.1. Liquid-crystalline MIPs synthesis

In their protocol, Liu and Mosbach used EGDMA and 4-VP in an 85/15 mol/mol ratio, with EGDMA acting as a crosslinker and 4-VP as a functional monomer. In order to assess the influence of liquid-crystalline groups on the catalysis properties, we used the liquid-crystalline monomer MAC6OMe in a 73 mol% ratio leaving the percentage of 4-VP unchanged (Table 1). The synthesis of LC-MIP is described in Scheme 3. As the polymerisation and crosslinking step was planned to be carried out at 4°C under UV irradiation as in Liu and Mosbach's article (*8*), preliminary experiments were performed to verify that none of the molecules besides the initiator absorbed in the chosen UV irradiation range, i.e. at wavelengths higher than 335 nm. Furthermore, poly(MAC6OMe) was also synthesised under these conditions to ensure that its reactivity was good enough in photopolymerisation. It was obtained in 80% yield after 7 h of irradiation, which was acceptable.

Based on these preliminary experiments, MIPs were synthesised under the conditions reported in Table 1.

MIP synthesis: CH_2Cl_2, EGDMA and 4-VP were degassed for 30 min before use. Then 198 mg of MAC6OMe (0.48 mmol), 11 mg of 4-VP (0.102 mmol), 15 mg of EGDMA (0.077 mmol), 1.8 mg of indole (0.015 mmol) and 50 µl of methylene chloride were mixed in a Teflon beaker, which was placed in an argon-purged vessel. The mixture was left for 2 h at 4°C for the preorganisation part. This delay was chosen based on preliminary characterisation of the complex between indole and 4-VP, for which a one-to-one stoechiometry was found with a weak affinity constant of 1.2 M^{-1} (see supplementary information available online). Next 1.6 mg of AIBN (0.01 mmol) was introduced in 50 µl CH_2Cl_2. A new purge was performed for 10 min. The set-up was then irradiated at 4°C for 7 h. Non-imprinted polymers were synthesised in the same manner without indole. The polymers were washed with successive MeOH/acetic acid 9/1 solutions until no signal in UV spectroscopy could be detected and then rinsed twice with pure methanol to eliminate any trace of acetic acid. The washing solutions were characterised by HPLC (Waters Alliance 2695, UV detector at 270 nm, XTerra RP18 column, eluent water/acetonitrile 55/45). The mass of extracted products was close to 30% of the initial weight. NMR analysis of the extracted solutions showed that it consisted, besides indole, of EGDMA and MAC6OMe in a 1/5.7 ratio. This showed that both monomers reacted similarly because the initial ratio between EGDMA and MAC6OMe was 1/6.1. No 4-VP could be detected, proving its complete reaction. HPLC analysis of the extracted solutions showed that 90% of the initial indole was removed from the material. For the non-liquid-crystalline materials, the quantity of extracted molecules was lower, typically close to 9%, which was consistent with Liu and Mosbach's results. In this case, both EGDMA and 4-VP were recovered in the washing solutions, as well as indole for MIP-0.

Liquid-crystalline MIPs were characterised by DSC and presented a glass transition at 54.6°C and an isotropic to mesomorphic transition at 107°C (see

Table 1. Composition of the synthesised materials.

Polymer	EGDMA (mol%)	HDMA (mol%)	MAC6OMe or MAC6CN (mol%)	4-VP (mol%)	[4-VP]/[Indole]
MIP-0	85	—	—	15	6.8
NIP-0	85	—	—	15	—
LC-MIP-1	12	—	73	15	6.8
LC-NIP-1	12	—	73	15	—
MIP-s-IPN-1	14	—	70	16	6.8
NIP-s-IPN-1	14	—	70	16	—
MIP-s-IPN-2	—	14	70	16	6.8
NIP-s-IPN-2	—	14	70	16	—

supplementary information available online). The polymers were then crushed and sieved and the particles, the diameters of which were between 25 and 75 µm, were used for the kinetic tests. The particles with smaller diameters were used for DSC characterisations and those with larger diameters for SEM experiments.

2.3.2. *S-IPN synthesis*

The s-IPNs were synthesised in a two-step procedure depicted in Scheme 4. In a first step, a copolymer of 82 mol% MAC6CN and 18 mol% 4-VP was obtained by classical radical polymerisation initiated by AIBN. In a second step, this polymer was dissolved in a solution containing a difunctional methacrylate monomer (either EGDMA or hexadecylmethacrylate (HDMA)), indole and AIBN (Table 1). The 4-VP/indole ratio was fixed at 6.8 to optimise the quantity of complex formed during the synthesis.

Synthesis of the liquid-crystalline polymer poly(MAC6CN-co-4-VP): Toluene and 4-VP were degassed before use. Then 1.5 g of MAC6CN (4.13 mmol), 93 mg of 4-VP (0.884 mmol) and 20 mg of AIBN (0.123 mmol) were dissolved in 2 ml of toluene in a ground flask. The system was degassed and then stirred at 70°C for 24 h in the dark. 1.56 g of yellowish polymer was obtained. Analysis by size exclusion chromatography gave a mean molar mass $\overline{M_w}$ of 59,700 g mol^{-1}. ^{1}H NMR (500 MHz): 0.91–1.77 (m, –CH_2– and Me–); 3.94 (m, –CH_2–O–; 6.47 (m, CH_{Ar}(4-VP) β from N); 6.93 (m, CH_{Ar}(biphenyl) β from –O–); 7.47 (m, CH_{Ar}(biphenyl) β from –Ph–CN); 7.58 (m, CH_{Ar}(biphenyl) β from –CN); 7.63 (m, CH_{Ar}(biphenyl) β from –CH_2O–Ph); 8.41 (m, CH_{Ar}(4-VP) α from N). ^{13}C NMR (400 MHz): 23.46 (CH chain); 25.8 (–CH_2– γ from –O–); 25.9 (–CH_2–); 28.1 (–CH_2– β from ester group); 29.1 (–CH_2– β from –O–Ph); 65.0 (–CH_2–OCO–); 67.8 (–CH_2–O–Ph); 110.1

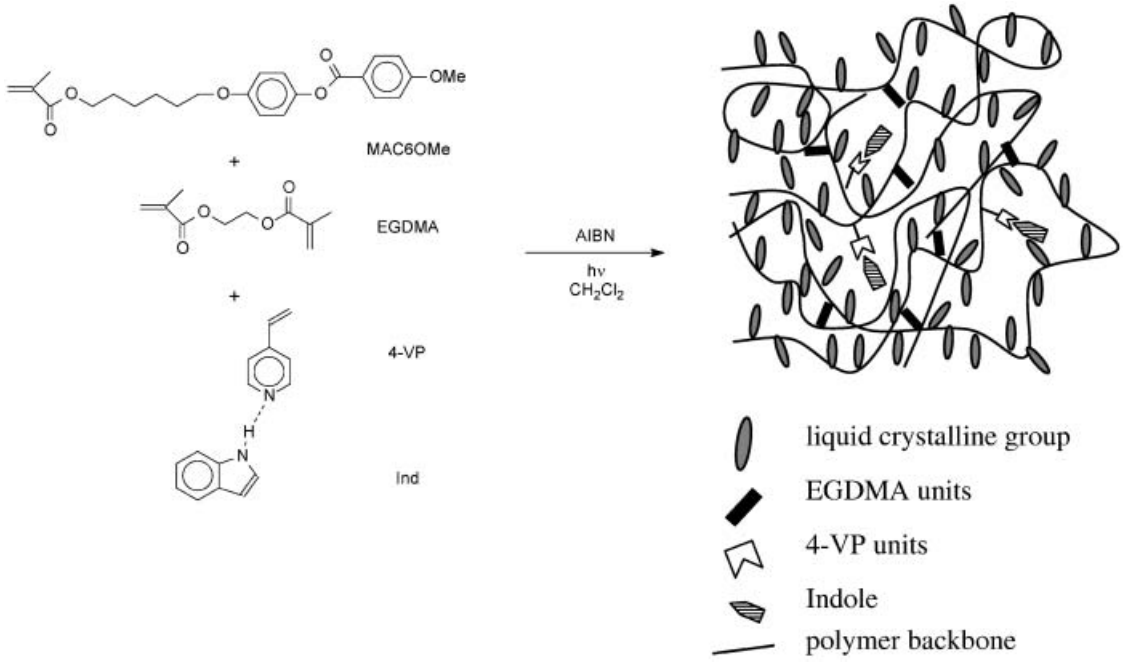

Scheme 3. Synthesis of the liquid-crystalline MIP.

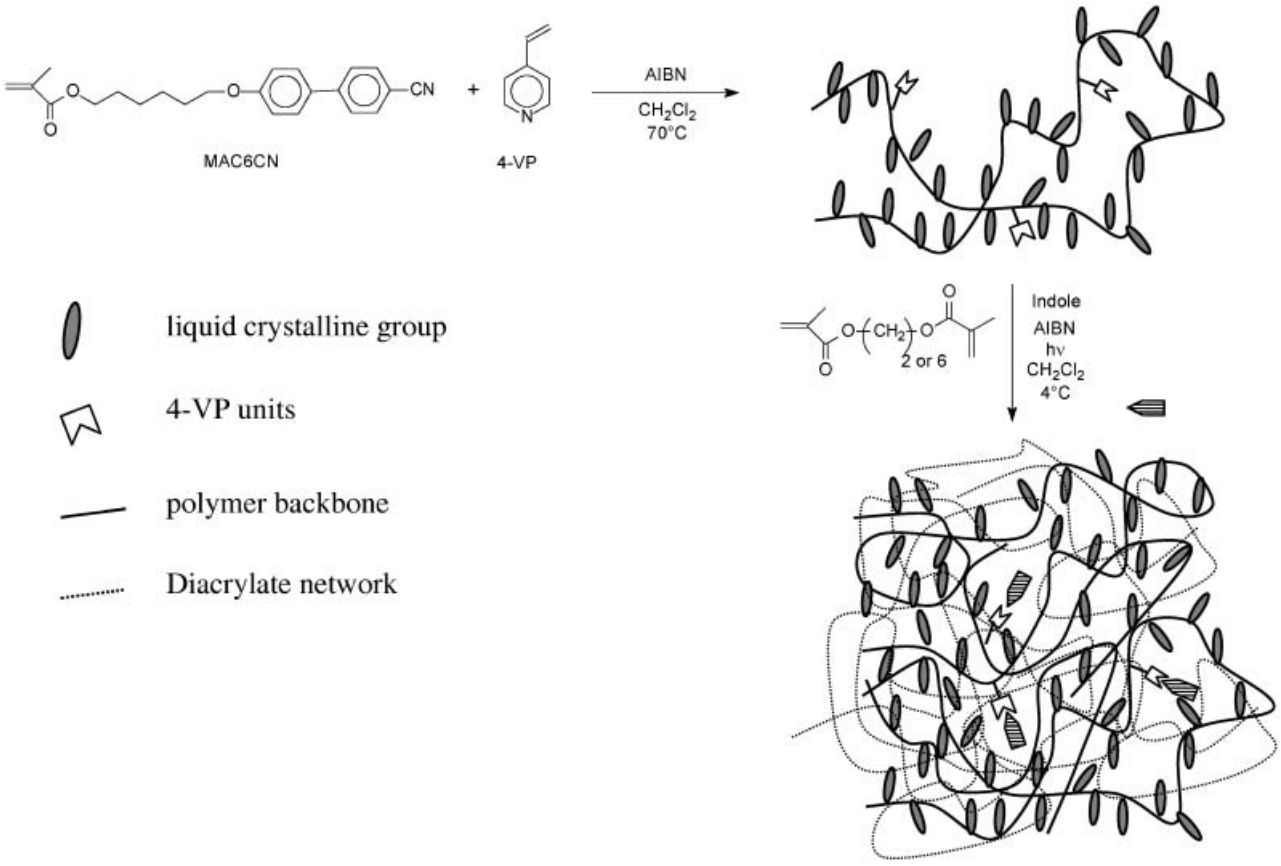

Scheme 4. Synthesis of the liquid-crystalline MIP-s-IPNs.

(C_{Ar} α from CN); 115.0 (–CH_{Ar}– β from –CH_2–O–); 119.0 (CN); 123.0 (CH_{Ar}(4-VP)); 127.2 (–CH_{Ar}– β from –Ph–CN); 128.3 (–CH_{Ar}– β from –CH_2–O–Ph); 131.3 (C_{Ar} α from Ph–CN); 132.6 (–CH_{Ar}– β from –CN); 144.9 (–CH_{Ar}– α from –CH_2–O–Ph); 159.6 (–C_{Ar}– α from –CH_2–O–); 168.5 (–COO–). Fourier transform infrared (FT-IR) spectra: 3069 cm^{-1} (ν_{CHAr}); 2224 cm^{-1} (ν_{CN}); 1724 cm^{-1} ($\nu_{COester}$); 1603–1472 cm^{-1} ($\nu_{C=C\ Ar}$). DSC: isotropic to smectic A (based on POM observations) transition at 105°C, T_g=56°C (see supplementary information available online).

s-IPN-MIP synthesis: CH_2Cl_2 and EGDMA (respectively, HDMA) were degassed for 30 min before use. Then 208 mg of poly(MAC6CN-co-4-VP), 26 mg of EGDMA (respectively, 35 mg of HDMA) (0.132 mmol), 2.0 mg of indole (0.017 mmol) and 0.5 ml of methylene chloride were mixed in a Teflon beaker, which was placed in an argon-purged vessel. The mixture was left for 2 h at 4°C for the preorganisation part. Then 1.6 mg of AIBN (0.01 mmol) was introduced in 0.2 ml CH_2Cl_2. A new purge was performed for 10 min. The set-up was then irradiated at 4°C for 7 h. Non-imprinted polymers were synthesised in the same manner without indole.

The polymers were washed with successive MeOH/acetic acid 9/1 solutions until no signal in UV spectroscopy in the rinsing solutions could be detected and then rinsed twice with pure methanol to eliminate any trace of acetic acid. Analysis of the rinsing solutions for s-IPNs either with EGDMA or HDMA only showed the extraction of indole without any other residual molecules. Typically, starting from 220 mg of material, 16 mg of product was extracted, consisting of 1.7 mg of indole and 14.3 mg of very fine particles of s-IPNs. With MIP-s-IPN-1 synthesised with EGDMA, we succeeded in removing only 60% of the imprint molecule in the washing steps and the first tests in kinetics revealed a very slow reaction, which could be attributed to a low accessibility of the active sites owing to the very dense network. Therefore, MIP-s-IPN-1 and NIP-s-IPN-1 were not further used in the kinetics. As for MIP-s-IPN-2 using the longer crosslinker HDMA, the extraction step led to the recovery of 75% of the imprint molecule. This shows that for s-IPNs, the effect of the crosslinker length is similar to regular networks. The recovery of 75% of the imprint molecule is less than what was observed for MIPs based on liquid-crystalline elastomers (*3*). This can be explained by the fact

that the present network is built only from the crosslinking agent. Therefore, it is denser than the regular elastomers. Non-imprinted s-IPNs were also synthesised following the same procedure without any indole added.

The polymers were then crushed and sieved and the particles, the diameters of which were between 25 and 75 µm, were used for the kinetic tests. The liquid-crystalline MIP-s-IPN-2 was characterised by DSC and presented a glass transition at 55°C and an isotropic to mesomorphic transition at 83°C (see supplementary information available online).

2.3.3. *Kinetic follow-up of benzisoxazole isomerisation*

After grounding and sieving, the polymer particles with sizes between 25 and 75 µm could be tested for catalysis of benzisoxazole isomerisation. To minimise the quantity of material used for each test, the procedure was slightly modified compared with Liu and Mosbach's paper (*8*). The reaction was followed by UV spectroscopy by recording absorbance both at 310 and 330 nm. These wavelengths were chosen so that the band of benzisoxazole (λ_{max}=284 nm in the reaction solvent) did not hamper the measurement of absorbance for 2-cyanophenol (λ_{max}=304 and 330 nm in the reaction solvent). The reaction was carried out directly in a UV cell with strong stirring, ensuring that no sedimentation of the polymer particles took place. As the reaction is base-catalysed, it is very sensitive to the solution pH. Furthermore, the UV spectrum of the product is also affected, because either 2-cyanophenol or 2-cyanophenolate could be formed depending on the pH. Therefore, all reactions were carried out at the same pH (a reading of 6.7 on the pH-meter) and both absorbances at 310 and 330 nm were recorded so that both forms of the product could be detected (Figure 1). Only the kinetics presenting similar ratios between these two bands were retained, ensuring that pH was exactly the same in all kinetics. The possibility of using buffer solutions for the kinetics was not followed since the introduction of various salts in the solutions would have lead to unknown responses of the materials therefore adding unknown parameters to the system.

A known weight of polymer particles (typically between 2.6 and 4.5 mg) was introduced in 2 ml of water/ethanol 3/1 vol/vol in a UV cell equipped with a magnetic bar. The suspension was stirred for 3 h before introduction of 0.25 ml indole solution ([Ind] between 0.5 and 3 mM). Absorbances at 310 and 330 nm were registered to follow the appearance of 2-cyanophenol. The optical densities were corrected for turbidity owing to the presence of particle suspension by subtracting the baseline level taken at 400 nm where no products absorbed. For the calculations, the extinction coefficient of 2-cyanophenol at 310 nm was measured in water/ethanol 3/1 and it was found at 1145 $cm^{-1} M^{-1}$.

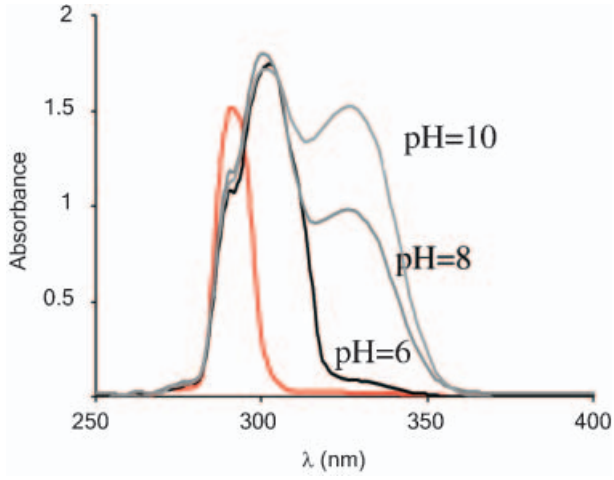

Figure 1. UV spectra of benzisoxazole and cyanophenol in water/ethanol 3/1 at various pH.

3. Results and discussion

The first part of the work dealt with a thorough characterisation of the complex between indole and the functional monomer 4-VP. This is reported in the supplementary information. All materials that have been synthesised are presented in Table 1 and the syntheses are detailed in the experimental part. Four different sets of materials were studied: an imprinted liquid-crystalline elastomer LC-MIP-1, two different s-IPNs MIP-s-IPN-1 and MIP-s-IPN-2 and, finally, a non-liquid-crystalline imprinted network MIP-0. LC-MIP-1 was obtained by using MAC6OMe and EGDMA as monomers. MIP-s-IPN-1 was obtained using MAC6CN as monomer and EDGMA as crosslinking agent, whereas MIP-s-IPN-2 used HDMA. MIP-0 corresponded to the MIP described by Liu and Mosbach (*8*) and was synthesised to compare the kinetics results between liquid-crystalline MIP and regular MIPs using exactly the same protocol. For all systems, non-imprinted polymers, LC-NIP-1, NIP-s-IPN-1, NIP-s-IPN-2 and NIP-0, were also obtained by performing the same synthesis without any indole. This means that these polymers contained 4-VP units in the same quantity as the MIPs, but lacked the imprinting effect.

During the synthesis, it was observed that only 60% of the imprint in MIP-s-IPN-1 could be withdrawn and early tests in kinetics showed that the catalysis of the reaction of benzisoxazole isomerisation by this material was very slow. This was attributed to the use of EGDMA as the crosslinking

agent for the network of the s-IPN, which in this case is very dense. Therefore, this material was not further used for the kinetics.

In order to benefit from the presence of liquid crystal in the elastomer, the materials had to be crosslinked in the mesomorphic state. This condition was mandatory to ensure that the formed elastomer presented a memory effect as predicted by De Gennes' theory (*35*). Thus, DSC measurements were carried out on the monomer mixtures just before irradiation. The solvent volume was adjusted so that the isotropic–liquid crystal transition was as close as possible to the reaction temperature set at 4°C. In the case of the liquid-crystal network LC-MIP-1, these tests showed that in the best conditions, the mixture was nematic for temperatures lower than −6.6°C (data not shown). This implied that the system was not liquid crystalline at the beginning of the reaction. However, because the transition temperature of liquid crystals increases rapidly with the molar mass, this guaranteed that the system quickly became liquid crystalline during the polymerisation.

This was confirmed by DSC experiments performed on the synthesised materials for LC-MIP-1 and MIP-s-IPN-2, which showed the presence of isotropic to mesomorphic transitions (see supplementary information available online). POM was unsuccessful, however, in further characterising the mesophases and X-ray experiments could not be performed at that time.

3.1. Characterisation of the materials by SEM experiments

SEM was performed in order to assess the porosity of the materials at least at the micrometer scale. The corresponding pictures are presented in Figure 2. A clear difference can be observed between non-liquid-crystal and liquid-crystal materials. Although synthesised with a comparable quantity of solvent, the former appear denser than the latter. This might be explained by the fact that for LC-MIPs, 30% of the monomers did not react and were recovered in the washing steps, versus 9% for MIP-0. MIP-s-IPN-1 appears denser compared with MIP-s-IPN-2. This corroborates the fact that the tests in catalysis with MIP-s-IPN-1 revealed a very slow reaction. The s-IPNs appear much more granular than the liquid-crystalline network LC-MIP-1. These pictures also showed that no difference could be observed between imprinted and non-imprinted analogues, even at higher magnification (data not shown).

3.2. Catalysis of benzisoxazole isomerisation

As the appearance of cyanophenol can be followed by UV spectroscopy, this technique was used for the kinetics. Typical evolutions of optical densities are presented in Figure 3. They all exhibited linear evolution on the entire range of the kinetic follow up, except for LC-MIP-1 which showed a slight curvature at the beginning.

In both liquid-crystalline and non-liquid-crystalline materials, an imprinting effect was observed, and the kinetic increase can be clearly seen in Figure 3 when comparing results for imprinted and non-imprinted materials of each type. For MIP-0 and NIP-0, the increase factor (calculated from the ratio of the slopes in Figure 3) was found close to 2.0, whereas for LC-MIP-1 and LC-NIP-1, this factor was close to 2.8. For the s-IPNs, a higher imprinting effect of 3.5 was calculated. This means that the cavity shape was well kept in the s-IPN, even if the functional monomers are not directly linked to the crosslinked system. As the SEM observations showed similar texture between imprinted and non-imprinted materials for each type of material, the observed increase in kinetics can truly be attributed to an imprinting effect.

It is worth noting that, in their article, Liu and Mosbach described an imprinting effect of 7 between imprinted and non-imprinted materials. The discrepancy between their value and the value found here could be attributed to the change in measurement set-up that we introduced for the kinetics. In Liu and Mosbach's article, only the absorbance of the solution part was measured through an on-line filtering system and a circulation between the reaction cell and the UV cell.

All materials exhibited a limited reaction rate at high substrate concentration, which is typical of enzymes. This saturation occurs when all active sites are used for the catalysis. Therefore, the kinetics were analysed according to Michaelis–Menten equations used for enzymes following the next reaction pathway and they were treated by Lineweaver–Burk plots according to the equation (*36*):

$$E + S \underset{k_{-1}}{\overset{k_1}{\rightleftharpoons}} E.S \xrightarrow{k_{cat}} E + P,$$

$$\frac{1}{V} = \frac{1}{V_M} + \frac{K_M}{V_M} \cdot \frac{1}{[S]},$$

with

$$K_M = \frac{k_{-1} + k_{cat}}{k_1},$$

where V is the initial rate of reaction and V_M is the maximal rate of reaction.

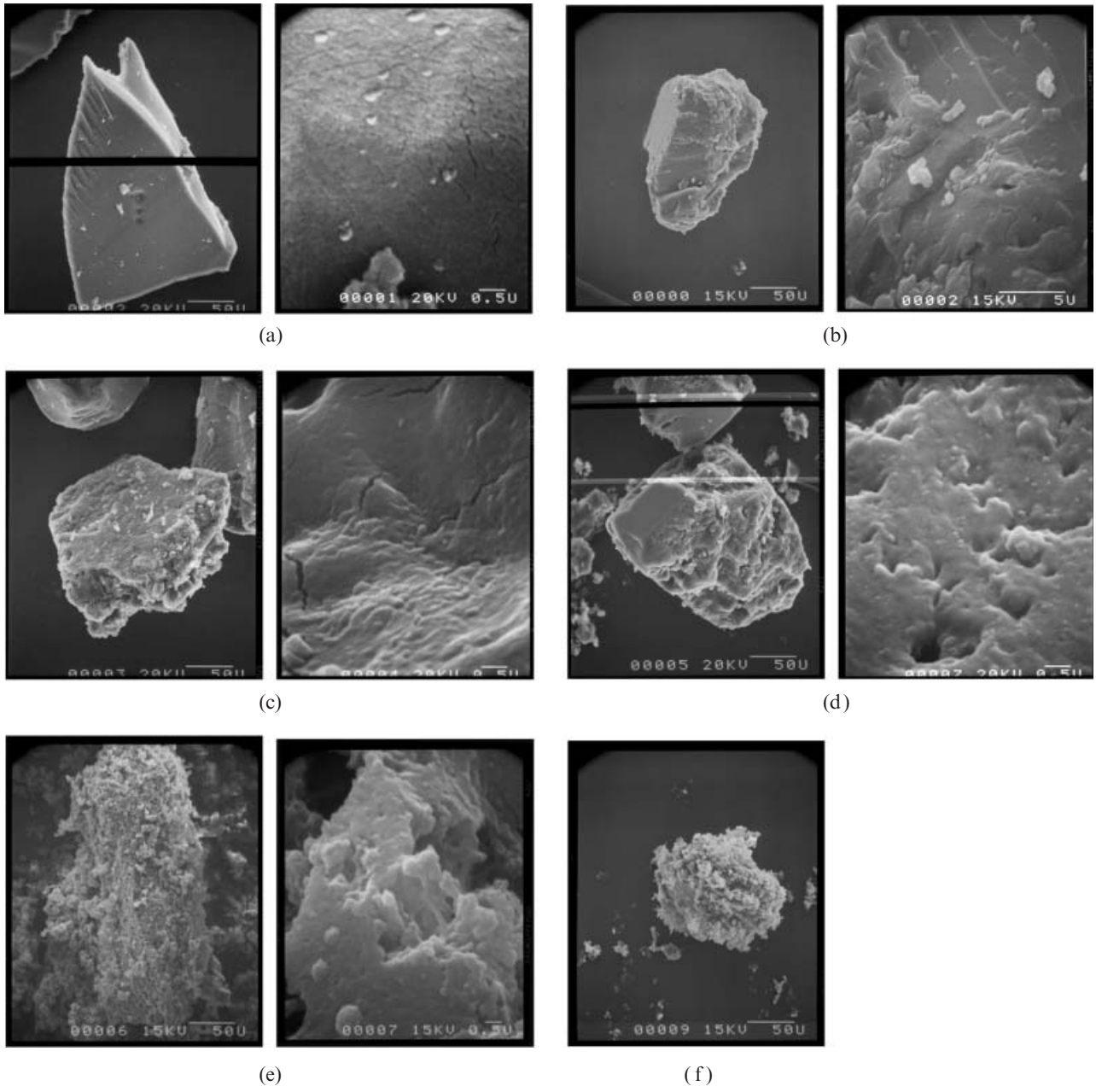

Figure 2. SEM micrographs: (a) MIP-0; (b) LC-MIP-1; (c) LC-NIP-1; (d) MIP-s-IPN-1; (e) MIP-s-IPN-2; (f) NIP-s-IPN-2. The white bar on the left in all pictures is 50 µm; the white bar on the right in (a), (b), (d) and (e) is 0.5 µm and in (c) is 5 µm.

The results are reported in Table 2 and Figure 4. Experiments were also carried out with MIP-0. Data from Liu and Mosbach's article (*8*) are also included in Table 2. For the non-imprinted materials, Lineweaver–Burk plots were not feasible because of very small evolutions of optical densities leading to too small a range of working concentrations for benzisoxazole.

Several comments can be made from these results. First, the obtained results for the kinetics for MIP-0 and 'MIP-0 Liu and Mosbach' are very different. As already explained, the experimental set-up for the kinetic follow-up was different in our procedure. Furthermore, we found that the reaction was extremely sensitive to differences in pH. However, in Liu and Mosbach's article, no such hint is discussed and thus the reactions may have not been performed under the same conditions. Another point is the range of benzisoxazole concentration used for the building of Lineweaver–Burk plot. Indeed, Liu and Mosbach used a wider range, from 0.07 to 1 mM, compared with 0.5–3 mM in our case. The too slow

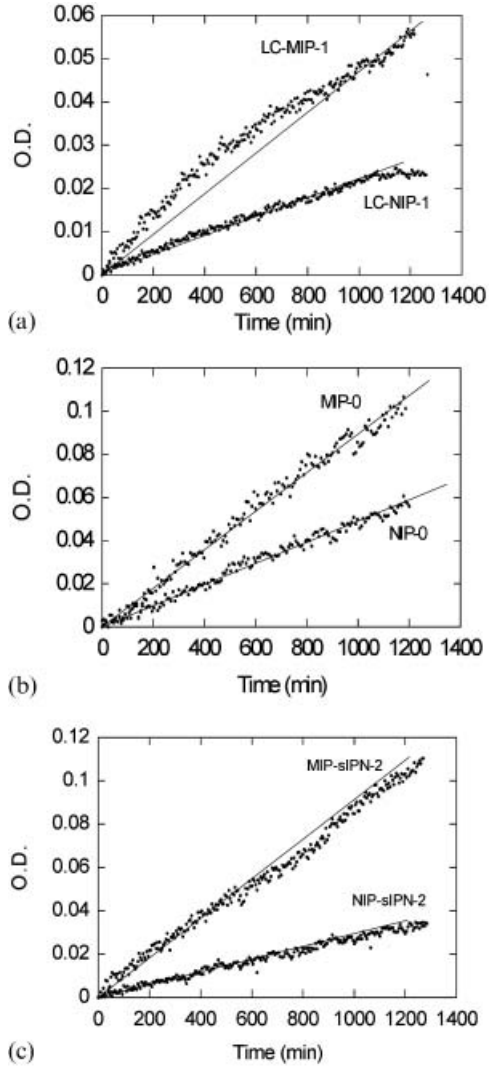

Figure 3. Typical evolution of optical densities for (a) liquid-crystal materials, (b) non-liquid-crystal materials and (c) s-IPNs. $[BziO]_0 = 3\,mM$, $[4\text{-VP}]_{Mat} = 0.89\,mM$, [Imprinted sites] $= 1.47 \times 10^{-4}\,M$.

reaction did not enable us to carry out the kinetic follow-up at lower concentrations. As a result, it does not seem reasonable to us to try and compare our results with those described by Liu and Mosbach. Consequently, we mainly focus the discussion on comparing MIP-0 with LC-MIP-1.

As K_M and k_{cat} are empirically defined constants, they are not related to any real property of the kinetic scheme. The parameter that should be considered and gives an idea of the catalytic efficiency of the enzyme is k_{cat}/K_M (see (*36*)). From this standpoint, both imprinted materials MIP-0 and LC-MIP-1 behave very similarly. On the other hand, the results show that MIP-s-IPN-2 exhibited a higher catalytic efficiency compared with a non-liquid-crystal MIP for which k_{cat}/K_M had a value of $0.25\,M^{-1}\,min^{-1}$.

However, one has to keep in mind that this global analysis following a Michaelis–Menten model is not rigorous in the case of MIPs, because only one type of active site is considered. A more thorough study should consider two types of active site: the imprinted sites (high-affinity sites) and the non-imprinted sites (low-affinity sites). Both are present in such MIPs because there is an excess of functional monomer versus imprint molecule during the synthesis. Such a dual Michaelis–Menten model exists, but many more kinetic follow-ups would be required to extract the appropriate constants for both types of site.

Another way to characterise the presence of and the difference in reactivities between imprinted and non-imprinted sites in the materials can be carried out by using the equilibrium constant that we determined and the quantities of each compound used in the synthesis. It is indeed possible to calculate the effective quantity of complex $n_{Ind.4\text{-}VP}$ formed which in turn leads to the quantity of imprinted sites in the final material. These values are presented in Table 3 for LC-MIP-1, MIP-s-IPN-2 and MIP-0. From these calculations, it can be shown that in the case of LC-MIP-1 and MIP-0, approximately 30% of the introduced indole molecules are really complexed to 4-VP, and approximately 4.5% of 4-VP is used in the complexes, owing to the low-affinity constant of the complex (see supplementary information available online). This means that in the final MIPs, the ratio of high-affinity/low-affinity sites is close to 4.5/95.5. For MIP-s-IPN-2, this ratio was even lower at 2.6/97.4. Knowing the percentage of complex in the MIPs, it is possible to compare the activity of both imprinted and non-imprinted sites in the isomerisation of benzisoxazole. To do this, the optical densities presented in Figure 3 are first corrected for the MIPs by retrieving the part due to the percentage of non-imprinted sites. These corrected optical densities enable a comparison of the slopes for a mole of imprinted sites versus a mole of non-imprinted sites (Table 4).

These calculations show that the imprinted sites of the s-IPN catalyse the reaction of isomerisation almost 100 times more compared with the non-imprinted sites. These results are undeniably better than those obtained for non-liquid-crystal MIP for which the imprinted sites catalysed the reaction 22 times more compared with the non-imprinted sites. For LC-MIP-1, the result is in-between, because the imprinted sites are 37 times more active than the non-imprinted sites.

It could be argued that we have compared imprinted systems with non-imprinted systems synthesised without any template molecule at all. By doing this, the porosity at the molecule scale is

Table 2. Kinetics parameters for the isomerisation of benzisoxazole ([*E*] is the concentration of imprinted sites).

Polymer	K_M (mM)	V_M (mM min^{-1})	[*E*] (M)	k_{cat} (min^{-1})	k_{cat}/K_M (M^{-1} min^{-1})
LC-MIP-1	1.82	8.85×10^{-5}	1.47×10^{-4}	6.0×10^{-4}	0.33
MIP-0	2.14	8.01×10^{-5}	1.47×10^{-4}	5.4×10^{-4}	0.25
MIP-s-IPN-2	0.75	1.26×10^{-4}	1.47×10^{-4}	8.6×10^{-4}	1.15
Liu and Mosbach (*8*)	0.484	0.014	7.0×10^{-5}	0.205	424

lower for the non-imprinted systems, therefore leading to a lower reactivity in the catalysis process. A better method would have been to compare the imprinted systems with 'non-imprinted' systems synthesised using a non-functionalised template molecule leading to no interactions whatsoever, but providing approximately the same porosity. In our case, this would have meant the use of an aromatic molecule such as indene, as Liu and Mosbach described (*8*). In their article, Liu and Mosbach showed that both materials (without any print molecule or with indene) led to the same activity. Furthermore, what we are really interested in is not the imprinting factor by itself, but the comparison of these imprinting factors for liquid-crystal and classical MIPs.

3.3. *Shape memory characterisation*

An advantage of liquid-crystalline imprinted elastomers is also the possibility of using the memory effect of the mesomorphous material. This was predicted by De Gennes (*35*) and shown by Finkelmann and colleagues (*31, 37, 38*) and Keller and colleagues (*39, 40*). In such systems, a strong coupling between the liquid-crystalline moieties and the polymer backbone

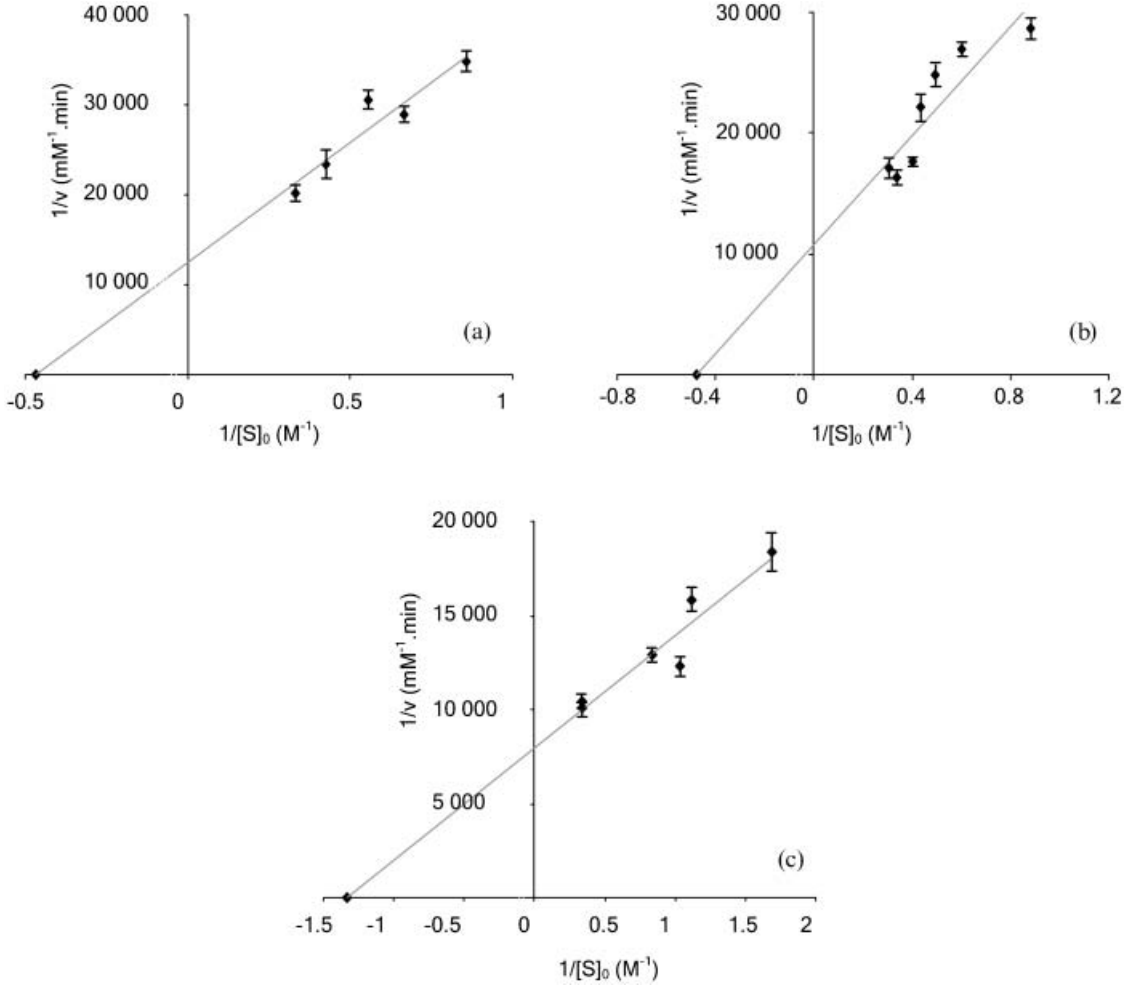

Figure 4. Lineweaver–Burk plots for (a) MIP-0, (b) LC-MIP-1 and (c) MIP-s-IPN-2.

Table 3. Characterisation of the complexing equilibrium during MIP syntheses (n_{Indole} and $n_{\text{4-VP}}$ are the mole number of indole and 4-VP, respectively, used in the synthesis; $n_{\text{Ind.4-VP}}$ is the mole number of complex between indole and 4-VP; $n_{\text{freeIndole}}$ and $n_{\text{free4-VP}}$ are the mole number of indole and 4-VP, respectively, not involved in the complex).

Polymer	n_{Indole} (mol)	$n_{\text{4-VP}}$ (mol)	Volume (l)	$n_{\text{Ind.4-VP}}$ (mol)	$n_{\text{freeIndole}}$ (mol)	$n_{\text{free4-VP}}$ (mol)
LC-MIP-1	1.54×10^{-5}	1.05×10^{-4}	2.76×10^{-4}	4.7×10^{-6}	1.07×10^{-5}	1.0×10^{-4}
MIP-s-IPN-2	1.7×10^{-5}	1.16×10^{-4}	7.37×10^{-4}	2.64×10^{-6}	1.44×10^{-5}	1.13×10^{-4}
MIP-0	1.7×10^{-4}	1.11×10^{-3}	3.4×10^{-3}	4.65×10^{-5}	1.23×10^{-4}	1.06×10^{-3}

Table 4. Comparison of reactivities between imprinted and non-imprinted sites (v_{corr} is reaction rate of each site calculated per site and after removal of the percentage due to non-imprinted sites; $v_{\text{impr}}/v_{\text{non-impr}}$ is the ratio of v_{corr} for the imprinted sites over v_{corr} for the non-imprinted sites).

Polymer	$[\text{4-VP}]_{\text{Mat}}$ (M)	Imprinted sites (M)	Non-imprinted sites (M)	v_{corr} (per site molel^{-1}-min^{-1})	$v_{\text{impr}}/v_{\text{non-impr}}$
LC-MIP-1	0.89×10^{-3}	4.41×10^{-5}	8.50×10^{-4}	0.96	36.8
LC-NIP-1	0.89×10^{-3}	—	0.89×10^{-3}	0.026	
MIP-s-IPN-2	0.89×10^{-3}	2.35×10^{-5}	8.70×10^{-4}	2.84	98.1
NIP-s-IPN-2	0.89×10^{-3}	—	0.89×10^{-3}	0.029	
MIP-0	0.89×10^{-3}	3.97×10^{-5}	8.50×10^{-4}	1.2	22.4
NIP-0	0.89×10^{-3}	—	0.89×10^{-3}	0.053	

exists ensuring that if the elastomer is formed in the mesomorphic phase, the interactions between the liquid crystals impose a permanent arrangement of the backbone's conformation to which the material will come back whenever possible. This has been studied and characterised at the macroscopic scale on monodomain materials heated above the clearing temperature or deformed by mechanical stress. However, no study has so far described what happens at the molecular level. In the field of materials with specific molecular recognition abilities, it seemed an important challenge to examine such a question.

A first way of characterising this was carried out through a thermal treatment. Thus, LC-MIP-1 was heated to 120°C, which is much higher than the mesomorphous–isotropic at 55°C, leading to a complete disorganisation of the liquid-crystalline moieties and therefore deformation of the cavities. The sample was then cooled back to room temperature and benzisoxazole isomerisation was carried out again. The corresponding kinetics curves are represented in Figure 5. Both curves, obtained before and after thermal treatment, are superimposed. The imprinted sites have therefore recovered their initial shape completely.

In addition to disorganisation by thermal treatment, the influence of mechanical deformation by swelling was also studied. This was carried out by synthesising LC-MIP-2 in the same manner as LC-MIP-1, but the washing steps were carried out with methylenechloride, which considerably swells the material. The corresponding curves presented in Figure 5 show that LC-MIP-2 was able to catalyse the reaction at the same rate as LC-MIP-1. Therefore, the network was able to swell and unswell while exactly recovering the shape of the cavities that had been formed in the MIP. For comparison, Figure 6 shows the evolution of the kinetics performed with MIP-0 before and after the same treatment. In this case, the kinetics after CH_2Cl_2 swelling were very slow, even slower than the kinetics with NIP-0, showing a complete deformation of the cavities. Shape memory properties were also examined for MIP-s-IPN-2 and revealed that no clear memory was present, even if the cavities were not completely deformed. This corroborates the fact that shape memory can exist only when a strong coupling between the three-dimensional network and the mesogenic groups is present.

4. Conclusion

In this study we have aimed at characterising the influence of liquid-crystal moieties in MIPs used for catalysis. In previous articles, we had already shown that LC-MIPs enabled us to considerably lower the crosslinking agent percentage, therefore leading to higher accessibility to the sites and higher mass capacity of the materials. In this article, we have further shown that LC-MIPs could be used successfully in MIPs synthesised around a transition-state analogue, leading to analogues of enzymes. We have demonstrated that even with very small complex formation constants, imprinting effects can be observed. If the imprinting effect of non-liquid-crystal and liquid-crystal MIPs are similar, the main advantage of LC-MIPs is the shape memory property, because we have shown that these materials

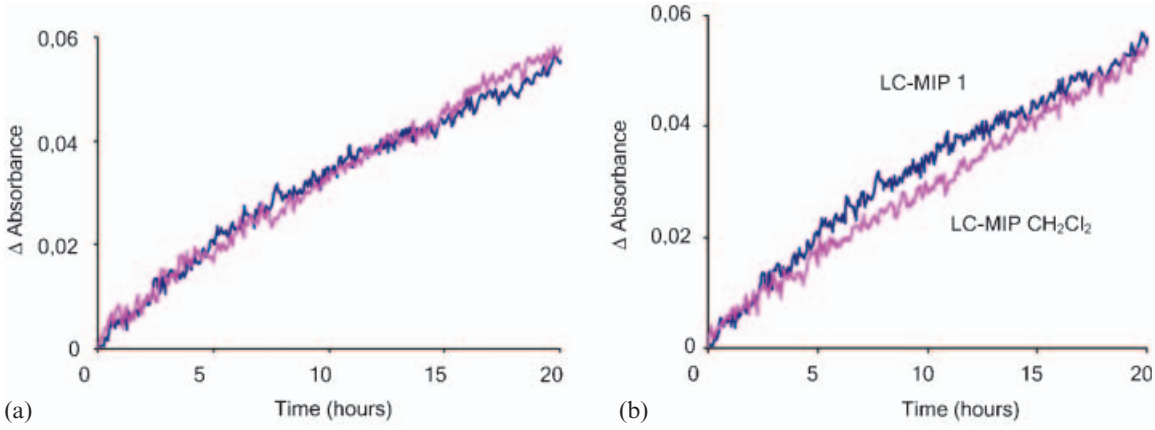

Figure 5. Shape memory characterisation of LC-MIP-1. (a) Kinetics before and after thermal treatment. (b) Kinetics before and after swelling with methylenechloride.

catalyse the chosen reaction at exactly the same rate, even after complete disorganisation of the cavity through thermal treatment or solvent-induced swelling.

Moreover, we have also shown for the first time that imprinted liquid crystalline s-IPNs could be synthesised and used as synthetic enzymes. An imprinting factor of 3.5 between the imprinted and the non-imprinted materials has been evaluated and is in the most often found range for regular MIPs. By comparing the kinetic curves of each system, we have shown that the imprinted sites in s-IPNs were much more active than the non-imprinted sites and that the difference in reactivities is much higher compared with classical non-liquid-crystal MIPs. The results presented here show that imprinted liquid-crystalline s-IPNs present a high accessibility to the active sites compared with the regular MIPs. This brings two types of questions regarding, first, the liquid-crystal s-IPNs and, second, the catalysis properties of imprinted s-IPNs. De Gennes' theory on shape memory dealt with liquid-crystal elastomers (*35*). In the case here, no indication of such a property can be inferred. Indeed, tests of reusing the materials after thermal treatment or solvent-induced swelling revealed that the cavities could gain back, but only partially, their original shape. From another point of view, we have demonstrated that the imprinted sites of liquid-crystal s-IPNs are much more reactive compared with non-imprinted sites. Other catalytic systems should be synthesised in order to characterise whether this is a general fact for such materials or not.

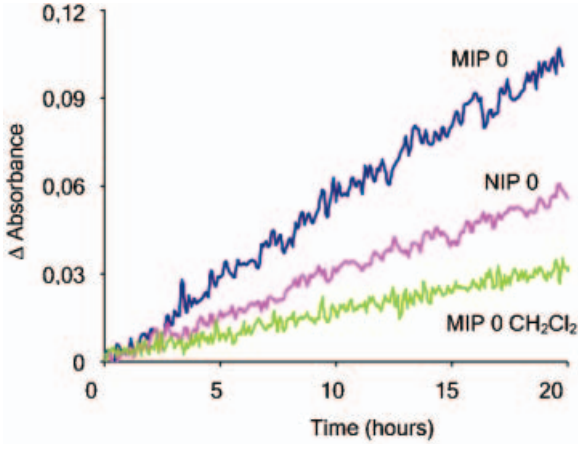

Figure 6. Evolution of kinetics for MIP-0 after methylenechloride swelling.

5. Supporting information available

Characterisations of the Indole/4-VP complex and DSC charts.

Acknowledgements

The authors wish to thank the French Ministry of Education and Research for a grant to M. Weyland. They also wish to thank P. Vicendo and C. Blonski for helpful discussions. Y. Chollet, P. Lavedan and C. Routaboul are acknowledged for their help in NMR and IR experiments. The Center of Electronic Microscopy Applied to Biology of the medicine faculty of Toulouse is also acknowledged for help with SEM experiments.

References

(1) Alexander C.; Andersson H.S.; Andersson L.I.; Ansell R.J.; Kirsch N.; Nicholls I.A.; O'Mahony J.; Whitcombe M.J. *J. Mol. Recogn.* **2006**, *19*, 106–180.
(2) Marty J.-D.; Mauzac M. *Adv. Polym. Sci.* **2005**, *172*, 1–35.

(3) Marty J.-D.; Mauzac M.; Fournier C.; Rico-Lattes I.; Lattes A. *Liq. Cryst.* **2002**, *29*, 529–536.
(4) Alexander C.; Davidson L.; Hayes W. *Tetrahedron* **2003**, *59*, 2025.
(5) Wulff G. *Chem. Rev.* **2002**, *102*, 1.
(6) Brüggemann O. *Anal. Chim. Acta* **2001**, *435*, 197.
(7) Beach J.V.; Shea K.J. *J. Am. Chem. Soc.* **1994**, *116*, 379.
(8) Liu J.; Mosbach K. *Macromol. Rapid Comm.* **1998**, *19*, 671.
(9) Visnjevski A.; Yilmaz E.; Brüggemann O. *Appl. Cat. A Gen.* **2004**, *260*, 169.
(10) Svenson J.; Zheng N.; Nicholls I.A. *J. Am. Chem. Soc.* **2004**, *126*, 8554–8560.
(11) Liu X.-C.; Mosbach K. *Macromol. Rapid Comm.* **1997**, *18*, 609.
(12) Biffis A.; Wulff G. *New J. Chem.* **2001**, *25*, 1537.
(13) Polborn K.; Severin K. *Chem. Eur. J.* **2000**, *6*, 4604.
(14) Locatelli F.; Gamez P.; Lemaire M. *J. Mol. Catal. A* **1998**, *135*, 89.
(15) Lettau K.; Warsinke A.; Laschewsky A.; Mosbach K.; Yilmaz E.; Scheller F.W. *Chem. Mater.* **2004**, *16*, 2745–2749.
(16) Liu J.; Wulff G. *Angew. Chem. Int. Ed. Engl.* **2004**, *43*, 1287.
(17) Liu J.; Wulff G. *J. Am. Chem. Soc.* **2004**, *126*, 7452.
(18) Sagawa T.; Togo K.; Miyahara C.; Ihara H.; Ohkubo K. *Anal. Chim. Acta* **2004**, *504*, 37.
(19) Sellergren B.; Karmalkar R.N.; Shea K.J. *J. Org. Chem.* **2000**, *65*, 4009.
(20) Kawanami Y.; Yunoki T.; Nakamura A.; Fujii K.; Umano K.; Yamauchi H.; Masuda K. *J. Mol. Catal. A* **1999**, *145*, 107.
(21) Ohkubo K.; Funakoshi Y.; Urata Y.; Hirota S.; Usui S.; Sagawa T. *J. Chem. Soc. Chem. Commun.* **1995**, *20*, 2143.
(22) Rich J.O.; Mozhaev V.V.; Dordick J.S.; Clark D.S.; Khmelnitsky Y.L. *J. Am. Chem. Soc.* **2002**, *124*, 5254.
(23) Liu J.; Luo G.; Gao S.Z.K.; Chen X.; Shen J. *J. Chem. Soc. Chem. Commun.* **1999**, *2*, 199.
(24) Sreenivasan K. *J. Appl. Polym. Sci.* **1998**, *70*, 19–22.
(25) Xia Y.-Q.; Guo T.-Y.; Song M.-D.; Zhang B.-H.; Zhang B.-L. *Biomacromolecules* **2005**, *6*, 2601–2606.
(26) Zhao X.; Du X.; Liu D.; Zhou Q. *Macromol. Mater. Eng.* **2000**, *274*, 36–41.
(27) Zhao X.; Hu X.; Yue C.Y.; Du X.; Zhou Q. *J. Appl. Polym. Sci.* **2000**, *76*, 1141–1150.
(28) Zhao X.Y.; Du Y.; Liu D.S.; Zhou Q.X. *J. Appl. Polym. Sci.* **1998**, *69*, 349–354.
(29) Fitzgerald J.; Noonan J.M.; Kapitza H.; Zentel R. *Polymer* **1991**, *32*, 2244–2251.
(30) Müller M.; Zentel R. *Macrmol. Chem. Phys.* **2000**, *201*, 2055–2063.
(31) Finkelmann H.; Wendorff J.H. *Makromol. Chem.* **1978**, *179*, 273.
(32) Shibaev V.P. *Eur. Polym. J.* **1982**, *18*, 651.
(33) Craig A.A. *Macromolecules* **1995**, *28*, 3617.
(34) Sasaki T.; Goto M.; Ishiwaka Y.; Yoshimi T. *J. Phys. Chem.* **1999**, *103*, 1925.
(35) De Gennes P.G. *Mol. Cryst. Liq. Cryst.* **1971**, *12*, 193.
(36) Stryer L. *Biochemistry*; Freeman: New York, 1981.
(37) Küpfer J.; Finkelmann H. *Makromol. Chem. Rapid Commun.* **1991**, *12*, 717.
(38) Kundler I.; Finkelmann H. *Macrmol. Chem. Phys.* **1998**, *199*, 677.
(39) Thomsen D.L. III.; Keller P.; Naciri J.; Pink R.; Jeon H.; Shenoy D.; Ratna B. *Macromolecules* **2001**, *34*, 5868.
(40) Naciri J.; Srinivasan A.; Jeon H.; Nikolov N.; Keller P.; Ratna B. *Macromolecules* **2003**, *36*, 8499–8505.